Multiphysical Time- and Frequency-Domain Fault Detection and Isolation Technique for Power-Electronic Converters in DFIG Wind Turbines

Marcelo Nesci Soares, *Member, IEEE*, Yves Mollet, *Member, IEEE*, Michel Kinnaert, *Member, IEEE*, Johan Gyselinck, *Member, IEEE*, and Jan Helsen, *Member, IEEE*

***Abstract*—A multiphysical time- and frequency-domain fault detection and isolation method for power-electronic converters of wind turbines is presented in this article, with focus on open-circuit faults in doubly-fed induction generator drivetrain topology. In order to reduce the risk of false alarms, the proposed approach combines fault indicators based on a time- and frequency-domain analysis of electrical signals, as well as a frequency-domain analysis of vibration signals. The effectiveness of the method is demonstrated via test bench data recorded under different healthy and faulty operating conditions.**

***Index Terms*—Condition monitoring, doubly-fed induction generator (DFIG), fault diagnostic and isolation, open-circuit faults, power electronic converter (PEC), semiconductor reliability, wind turbines (WT).**

I. Introduction

WIND turbine (WT) reliability and its effect on operation and maintenance costs are today a major concern both to WT manufacturers and wind-farm operators. Due to the increasing power rating of WTs and their use in harsher environments (e.g., offshore wind farms), the reliability of the components is seen as a critical issue for WT operation. Consequently, predictive maintenance based on condition monitoring has been shown as the most efficient maintenance strategy for WTs in order to reduce the operating costs and achieve economic viability [1].

The doubly-fed induction generator (DFIG) remains to date the most commonly used generator for variable-speed WTs. The associated power-electronic converter (PEC) is typically sized at only 30% of the rated generator power, which comes with lower cost and losses, and higher compactness, while allowing for variable speed, maximum power extraction from the wind, control of the exchange of active and reactive power with the grid, and reduced fatigue loading [2].

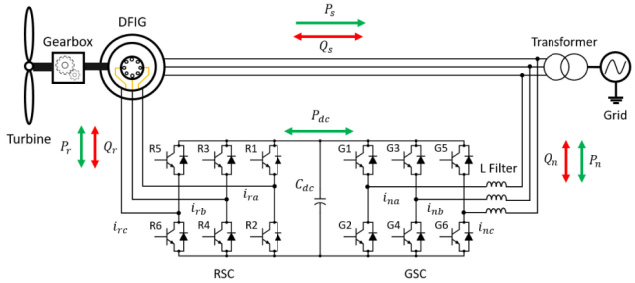

Fig. 1. DFIG WT topology.

Fig. 1 shows the DFIG WT topology. The three-phase ac/dc/ac PEC comprises two voltage-source converters, mounted back-to-back with common dc bus. The stator winding of the DFIG is directly connected to the 50 Hz (or 60 Hz) grid directly (via a transformer). The rotor-side converter (RSC) and the grid-side converter (GSC) are connected to the rotor winding of the DFIG and to the grid, respectively. The rotor currents have an ever changing fundamental frequency given wind speed and, hence, rotational speed variation; this is a complication for the detection of faults in the RSC, which furthermore affect more directly the rest of the WT. The detection of faults in the GSC is less challenging given the constant frequency. We therefore focus on RSC faults, noting that the proposed techniques can be applied straightforwardly to GSC faults.

The PEC is known to be one of the most reliability-critical components of a WT, with a share of around 25% of the failures and 14% of the overall downtime [3]. Inside the PEC, the semiconductors (or power switches) are the biggest cause of failures, besides capacitors, gate drivers, connectors, and inductors [4]. For DFIG WTs, the insulated-gate bipolar transistor (IGBT) is commonly used [5]; they are subject to thermal cycling due to load variation, fluctuating ambient temperature, and periodical commutation [6]. Switch failures can be mainly classified into short- and open circuits. IGBT short circuits are destructive in nature and, hence, readily detected by hardware protection circuits present in the PEC. Open-circuit faults have relatively mild electrical and mechanical consequences (overcurrent and thermal stress, distorted current waveforms, three-phase unbalance

Manuscript received January 31, 2020; revised July 23, 2020; accepted August 21, 2020. Date of publication September 2, 2020; date of current version November 20, 2020. Recommended for publication by Associate Editor Z. Chen. *(Corresponding author: Marcelo Nesci Soares.)*

Marcelo Nesci Soares is with the Federal Center of Technological Education "Celso Suckow da Fonseca" (CEFET/RJ), Rio de Janeiro 20271-204, Brazil, with the Universisité Libre de Bruxelles, 1050 Brussels, Belgium, and also with the Vrije Universiteit Brussel, 1050 Brussels, Belgium (e-mail: marcelonesci@poli.ufrj.br).

Yves Mollet and Johan Gyselinck are with the Bio, Electro, and Mechanical Systems Department, Université Libre de Bruxelles, 1050 Brussels, Belgium (e-mail: yves.mollet@ulb.ac.be; johan.gyselinck@ulb.ac.be).

Michel Kinnaert is with the Department of Control Engineering and System Analysis, Université Libre de Bruxelles, 1050 Brussels, Belgium (e-mail: michel.kinnaert@ulb.ac.be).

Jan Helsen is with the Acoustics & Vibration Research Group, Vrije Universiteit Brussel, 1050 Brussels, Belgium (e-mail: jan.helsen@vub.be).

Color versions of one or more of the figures in this article are available online at https://ieeexplore.ieee.org.

Digital Object Identifier 10.1109/TPEL.2020.3021306

and power/torque oscillations), such that the WT can remain operating during an extended period of time without detecting of the fault. Nevertheless, early detection of open-circuit faults is important for reducing unfavorable loading and, thus avoiding secondary faults in the converter or other components. An open-circuit fault can be divided as open-switch or open-phase fault. Both are generated by IGBT module failure or from the misfiring of the gates drivers; however, different from open-switch, an open-phase fault is characterized by having two defective IGBTs in the same PEC leg.

Many techniques have been developed to detect and isolate IGBT open-circuit faults for different WT topologies using electrical signals [7]–[9]. However, since the majority of these works mainly rely on current signature analysis, the developed techniques are sensitive to nonstationary operating conditions of the WT and can lead to a substantial rate of false alarms and nondetected faults. In order to remedy these issues, a model-based open-circuit fault detection technique has been proposed in [10], but at the expense of a higher computational cost and the need of accurate knowledge of the machine parameters. Another technique proposed in [11] investigates the dc-link voltage signal by time-domain (TD) and frequency-domain (FD) using wavelet technique to detect PEC open-circuit fault. No analysis regarding the robustness of the algorithm under healthy transient cases is shown. This technique is capable of detecting the fault but hardware-reconfiguration or fault-tolerant control is not recommended since no isolation capabilities are provided to localize the faulty converter leg. Wavelet techniques typically require more input parameters and successive decomposition levels by filter banks to achieve a reasonable frequency resolution.

Faults in the RSC also affect the vibration signature of the generator and, thus, the complete drivetrain. Accelerometers are already placed on the housing of the gearbox or generator in most modern WTs in order to detect faults in gears, bearings, or shafts by monitoring mechanical vibration signatures, for which a whole range of techniques is available [12]. The detection of rotor bar failures in squirrel-cage induction machines via TD and FD vibration analysis is widely researched [13]; but to our knowledge, no studies have been published regarding PEC open-circuit faults.

In order to solve the issues related to open-circuit faults in DFIGs WT, a novel robust FDI technique based on the fusion of electrical and mechanical signals and the combination of TD and FD analysis approaches is proposed. The combinations of both algorithms, working in parallel, seek to increase the reliability. The TD FDI technique, object of Section II, stems from the combination of a statistical approach based on the cumulative sum (CUSUM) algorithm and a signal-based technique to detect and isolate the fault, respectively. Regarding the FD fault detection technique, the autopower spectrum of the vibration, mechanical speed, and current signals are exploited and relevant fault indicators are determined in Section III. The logic for the combination of the TD and FD methods is presented in Section IV. Finally, experimental results are reported on the 3-kW 4-pole DFIG test bench in Section V.

II. TD FDI Technique

Aiming to mitigate the amount of false alarms and undetected faults, the proposed TD FDI technique combines a statistical CUSUM algorithm, monitoring the variance of the reactive power and a signal-based algorithm, monitoring the converter currents. While the former detects the presence of a fault, the latter locates a possibly faulty IGBT.

TABLE I
Stator Reactive Power Statistical Parameters Under Open-Circuit Faults

Statistical Parameters [var]	μ_o	σ_0	μ_1	σ_1
Open-Switch				
	8 Nm			
1300 rpm	449.6	30.6	451.3	989.6
1600 rpm	449.6	30.4	446.6	1107.7
	12 Nm			
1300 rpm	449.8	31.1	449.3	1026.8
1600 rpm	449.6	31.2	505.1	1201
Open-Phase				
	8 Nm			
1300 rpm	449.5	28.6	450	1410
1600 rpm	449.7	31.6	764.6	1633.5
	12 Nm			
1300 rpm	449.7	31.2	449.6	1270.1
1600 rpm	449.7	31.7	886.7	1719.4

A. Fault Detection Based on CUSUM Algorithm

The reactive power usually stays constant and is controlled by the PEC, regardless of the DFIGs operating condition. Normally this value is controlled to be as close as possible to zero in order to maintain the unitary power factor at the grid connection [14]. Furthermore, according to the work in [15], the occurrence of an open-circuit fault on WECS can result in a huge fluctuation of the electromagnetic torque, generator speed, and reactive power. This is illustrated in Table I, which provides the mean and variance of the reactive power signal recorded on the 3-kW DFIG test bench presented in Section V under different operating conditions and open-circuit faults. μ_0 and σ_0 (μ_1 and σ_1), respectively, correspond to the mean and standard deviation of 1000 signal samples recorded at 150 Hz in healthy operation (under open-circuit operation). The stator reactive power is controlled to 450 var and for each value of rotating speed and torque, the standard deviation exhibits a huge change in the faulty case with respect to the healthy case while the change in the mean is much smaller. These huge changes in the standard deviation with limited change in the mean can be detected effectively online and with low computational cost thanks to the so-called CUSUM algorithm.

The algorithm relies on the log-likelihood ratio $s(Q_s)$ of an observation of the detection variable Q_s (stator reactive power), which is defined as

$$s(Q_s) = \ln \frac{p_{\sigma_1}(Q_s)}{p_{\sigma_0}(Q_s)} \tag{1}$$

where $p_{\sigma_0}(Q_s)$ and $p_{\sigma_1}(Q_s)$ denote the probability density function of Q_s under healthy and faulty conditions, respectively. $s(Q_s)$ is negative on average when the data correspond to the healthy model and positive on average when they correspond to the faulty mode. When p_{σ_0} and p_{σ_1} are perfectly known, this online algorithm provides the lowest mean detection delay for sufficiently large mean time between false alarms, which is a usual requirement [16]. However, in practice, the magnitude of the change is unknown and the signals might not be stationary. Nevertheless, even in such circumstances, the effectiveness of the algorithm has been checked in numerous applications [17],

[18]. The algorithm actually detects to which probability distribution the data samples are the closest. The CUSUM algorithm derived from the Gaussian distribution is the most widely used. The resulting log-likelihood ratio for detecting a change in the variance from σ_0 to σ_1 is

$$s(Q_s) = \ln\left(\frac{\sigma_0}{\sigma_1}\right) + \frac{(Q_s-\mu_0)^2}{2\sigma_0^2} - \frac{(Q_s-\mu_0)^2}{2\sigma_1^2}. \quad (2)$$

The CUSUM algorithm can be written in a compact recursive form as follows [19].

1) Initialization : set $g(0) = 0$
2) At the k^{th} sampling time:
   1) acquire the measurement $Q_s(k)$;
   2) compute the decision function $g(k) = \max(0, g(k-1) + s(Q_s(k)))$;
   3) if $g(k) > h$, generate an alarm and set the decision function $g(k)$ to 0.

In the aforementioned algorithm, h is a user-defined threshold that must be specified in order to achieve a reasonable tradeoff between fast fault detection and low false alarm rate. Upon occurrence of a fault, the algorithm thus generates repeated periodic alarms due to the reinitialization of the decision function in step 3.

B. Fault Isolation

The fault isolation algorithm evaluates the normalized absolute average values of currents and also the sign of the averaged currents. Due to the different WT operating conditions, the modulus of the three-phase currents is computed for normalizing the instantaneous current values in order to remove load and speed dependence [20].

The normalization is performed by dividing the absolute average values of the converter currents by the average modulus of the three-phase currents, as follows:

$$\delta_j(t) = \frac{\frac{1}{T}\int_{t-T}^{t} |i_j(\tau)| d\tau}{\frac{1}{T}\int_{t-T}^{t} \sqrt{\frac{2}{3}(i_a^2(\tau) + i_b^2(\tau) + i_c^2(\tau))} d\tau} \quad (3)$$

where $j \in \{a, b, c\}$, i_j is the instantaneous phase converter current, and T is the time-varying period of the signal.

Under healthy condition, the result of this computation presents a constant value equals 0.6366. Consequently, this value can be used as a reference for designing the value of the open-circuit fault isolation thresholds. For instance, during an open-switch fault, the current cannot flow anymore for half a period; hence, the magnitude of the relevant $\delta_j(t)$ is the half of the healthy value (0.3183). A similar reasoning leads to an ideal value of $\delta_j(t)$ equal to zero during a jth open-phase fault. Nevertheless, an open-switch or -phase fault due to a gate-driver failure, depending on the system operating point and electrical parameters, the parallel freewheeling diode of the IGBT may conduct part of the current. Hence, the magnitude of $\delta_j(t)$ in (3), during a gate driver failure, can be bigger than the ideal case. Therefore, after evaluating several operating points, and considering an open-circuit due to gate-driver failure as the most difficult case to isolate, the values of the fault isolation thresholds for open-switch and open-phase faults have been set to $\kappa_{\text{osw}} = 0.55$ and $\kappa_{\text{oph}} = 0.2$, respectively.

When an open-switch fault occurs on phase a, for instance, δ_a decreases, whereas the other two remaining δ_j ($j \neq a$) increase due to current unbalance on the electrical system.

TABLE II
DIAGNOSTIC SIGNATURES FOR FAULTY SWITCH IDENTIFICATION

Switch	Condition
S_1	If $\kappa_{oph} < \delta_a < \kappa_{osw}$ & $\overline{i_a} < 0$
S_2	If $\kappa_{oph} < \delta_a < \kappa_{osw}$ & $\overline{i_a} > 0$
S_3	If $\kappa_{oph} < \delta_b < \kappa_{osw}$ & $\overline{i_b} < 0$
S_4	If $\kappa_{oph} < \delta_b < \kappa_{osw}$ & $\overline{i_b} > 0$
S_5	If $\kappa_{oph} < \delta_c < \kappa_{osw}$ & $\overline{i_c} < 0$
S_6	If $\kappa_{oph} < \delta_c < \kappa_{osw}$ & $\overline{i_c} > 0$
S_1,S_2	If $\delta_a < \kappa_{oph}$
S_3,S_4	If $\delta_b < \kappa_{oph}$
S_5,S_6	If $\delta_c < \kappa_{oph}$

The algorithm summarized in Table II is able to determine which type of fault has occurred based on the magnitude of δ_j, $j \in \{a, b, c\}$, and its location based on the sign of the average currents. If the value of δ_j is lower than the threshold κ_{oph}, it implies that the system is subject to a jth open-phase fault. On the other hand, when the magnitude of δ_j is lower than the threshold κ_{osw} but higher than κ_{oph}, the system is experiencing an open-switch fault. Besides, since each converter phase is composed of two IGBTs, the sign of the average currents provides the location of the faulty IGBT.

III. FD FAULT DETECTION TECHNIQUE

The technique uses vibration, mechanical speed, and current data of the generator in the FD to develop a straightforward and robust fault detection scheme for converter open-circuit faults. During an open-circuit fault, for instance, in the RSC, several frequency side bands related with the rotor frequency can be detected in other system variables such as stator currents, generator speed, and vibration measurement. Similar observations can be seen in squirrel-cage machines in case of broken rotor bar or rotor unbalance [21]. The proposed FD fault detection algorithm aims at gathering both electrical and mechanical signals in order to improve the detectability. The output of the algorithm confirms or invalidates a faulty situation on the RSC. Therefore, the reliability of the final multiphysical TD and FD FDI algorithm increases when the output of both TD and FD algorithms accuses a faulty-mode.

A. Current Signature Analysis

The DFIGs stator currents are analyzed based on the envelope spectrum. Nowadays, envelope analysis is widely used for bearing diagnostics and widespread in the literature [22]. The developed envelope algorithm consists of demodulating the signal by squaring the input signal and then sending it through a low-pass filter [23]. In order to maintain the correct scale and the original signal energy, it is necessary to amplify the signal by a factor of two before low-pass filtering it. Moreover, it is necessary to reverse the scaling distortion by taking the square root of the signal after the low-pass filter [24].

In this article, a second order low-pass filter is used in the aforementioned procedure, with a cut-off frequency chosen in such a way that the frequencies amplified by an RSC failure are not attenuated by the filter. More precisely, the cut-off frequency is chosen below the fundamental stator frequency (50 Hz) and above the maximum fundamental rotor frequency (15 Hz) to

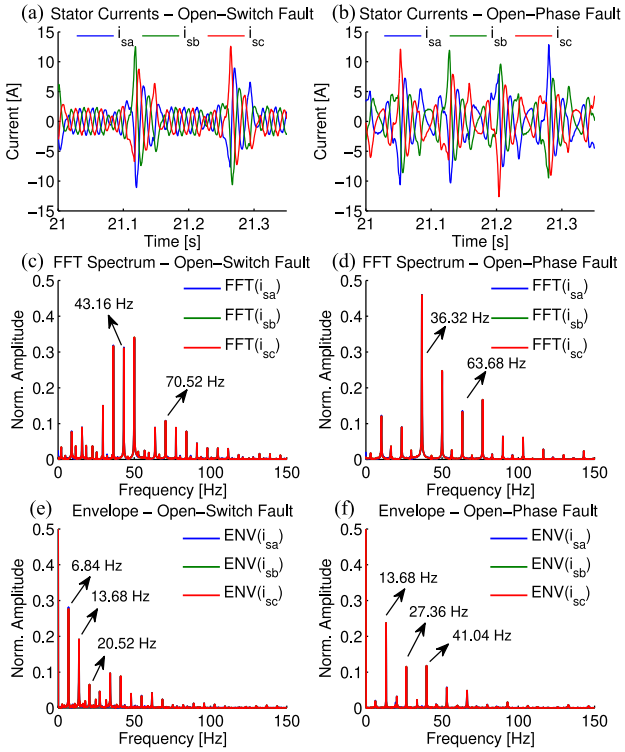

Fig. 2. Experimental results at 1295 r/min and 12 N·m. Stator current under (a) open-switch and (b) open-phase fault. FD analysis of the stator currents under (c) and (e) upper open-switch fault on phase C and (d) and (f) open-phase fault on phase C.

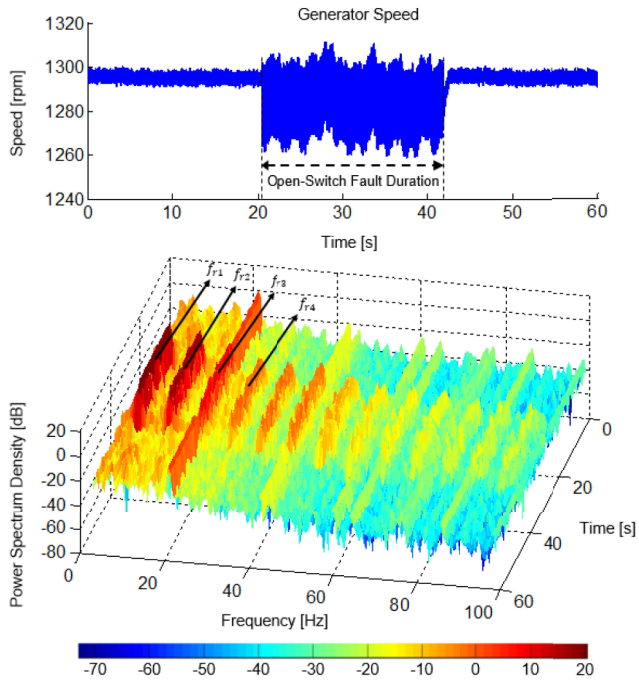

Fig. 3. Experimental results at 1295 r/min and 10 N·m. TD and FD analysis of the generator speed under an open-switch fault. Sampling frequency set to 5 kHz.

only keep the rotor frequency side bands. The chosen fundamental rotor frequency corresponds to the maximum slip operating condition for a DFIG topology (working with approximately 30% of slip). To obtain the envelope spectrum, a rectangular window of length K is applied to the signal processed as described in the first paragraph before computing its fast Fourier transform (FFT).

In order to facilitate the understanding, Fig. 2 shows the dynamics and the spectrum analysis of the stator currents during faulty condition (open switch and open phase) on the test rig.

Since the value of the mechanical speed is measured by the encoder, the slip of the machine can be determined from

$$s_{\text{slip}} = \frac{n_{\text{syn}} - n_{\text{mec}}}{n_{\text{syn}}} \tag{4}$$

where n_{syn} and n_{mec} are the synchronous and mechanical speed of the generator, respectively. Based on this, the values of the stator frequency peaks, during an open-switch and open-phase fault, can be computed as follows:

$$f_{\text{OSW}} = f_s.(\alpha \pm \gamma s_{\text{slip}}) \tag{5}$$

$$f_{\text{OPH}} = f_s.(\alpha \pm 2\gamma s_{\text{slip}}) \tag{6}$$

where f_s is the fundamental stator frequency, and α and γ are the stator and rotor harmonic orders, respectively.

In Fig. 2, side bands at the rotor harmonic order ($f_{r1} = 6.84$ Hz) appear in the FFT spectrum when an open-circuit fault occurs. Using the envelope spectrum analysis, the rotor frequency side bands ($f_{r\gamma} = f_s \cdot \gamma \cdot s_{\text{slip}}$) appear even more clearly. During a nonconstant operating condition, the slip is computed by considering the average value of the mechanical speed during the current rectangular window.

B. Vibration and Mechanical Speed Signature Analysis

Even in healthy condition, machines generate vibrations at frequencies directly linked to periodic events in the machine operation, such as rotating shafts, meshing gear teeth, rotating electric fields, etc., [12]. In this work, generator stator vibration and mechanical speed FFT analysis is performed during several WT operating conditions (healthy and faulty cases). In order to better understand the effects that a converter fault might generate to the mechanical system, Fig. 3 shows the spectrum analysis of the mechanical speed under an open-switch fault in the RSC on the 3-kW DFIG test bench. The dc component has been suppressed by a second-order high-pass filter.

Due to the speed of the generator (1295 r/min; $f_{\text{mech}} = 21.59$ Hz), the third harmonic order of the rotor frequency ($f_{r3} = 21.49$ Hz) is quite close to the mechanical frequency. A constant and high magnitude value of the power spectrum is observed at f_{r3} throughout all the experiment duration in Fig. 3.

C. Side-Band Fault Detection Technique

Figs. 2 and 3 clearly show the strong influence of a malfunction on the RSC since rotor sideband frequencies are observed on stator currents, vibration, and generator speed. In healthy operation, the spectrum at the sideband frequencies associated to faults has small magnitude compared its dominant peak present at the characteristic frequency of each specific variable (e.g., 50 Hz for the stator current). On the contrary, the spectrum magnitude at the side-band frequencies becomes comparable to its magnitude at the dominant peak frequencies in case of

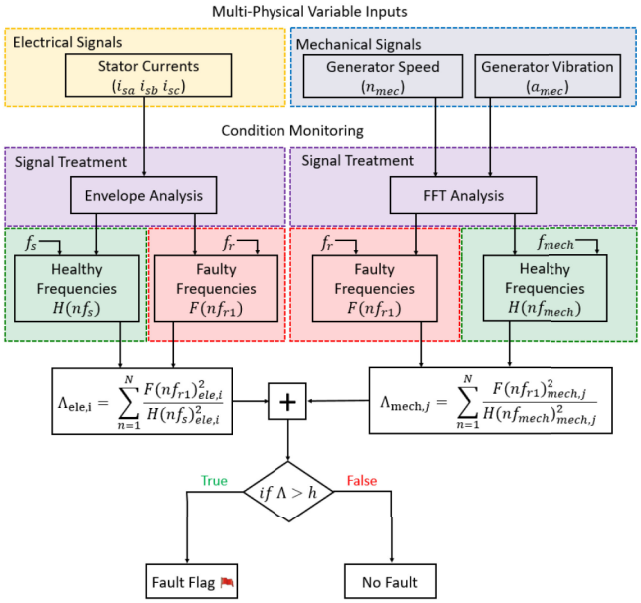

Fig. 4. FD fault detection algorithm.

fault. Therefore, the proposed fault detection algorithm aims to detect a fault based on the ratio of the component amplitudes of the spectrum at side-band frequencies and at the characteristic signal frequency. The fault indicators are computed according to the method depicted in Fig. 4. They can be formalized by

$$\Lambda_{\text{ele},i} = \frac{\sum_{n=1}^{N} F(nf_{r1})^2_{\text{ele},i}}{\sum_{n=1}^{N} H(nf_s)^2_{\text{ele},i}}, \qquad i \in \{a,b,c\} \quad (7)$$

$$\Lambda_{\text{mech},j} = \frac{\sum_{n=1}^{N} F(nf_{r1})^2_{\text{mech},j}}{\sum_{n=1}^{N} H(nf_{\text{mech}})^2_{\text{mech},j}}, \qquad j \in \{\omega, v\}, \quad (8)$$

where $F(nf_{r1})_{\text{elec},i}$ and $F(nf_{r1})_{\text{mech},j}$ denote the magnitude of the envelope and FFT, respectively, for the considered signal at the sideband frequency f_{r1} $(= f_s s_{\text{slip}})$, for $n = 1$ and its harmonics of order n (for $n = 2$ up to N). Similarly, $H(nf_s)_{\text{elec},i}$ and $H(nf_{\text{mech}})_{\text{mech},j}$ denote the magnitude of the envelope and FFT, respectively, for the considered signal at the characteristic signal frequency, namely the fundamental stator frequency (f_s) and the fundamental mechanical frequency according to the generator speed (f_{mech}). N is the highest analyzed harmonic order of the signal. $\Lambda_{\text{ele},i}$ are the fault indicators associated to the electrical signals with $i \in \{a,b,c\}$ corresponding to each stator current phase and $\Lambda_{\text{mech},j}$ are the fault indicators associated to the mechanical signals with $j \in \{\omega, v\}$. ω and v corresponds to the speed and vibration signals, respectively.

These five FD fault indicators are grouped into one global indicator denoted Λ defined as

$$\Lambda = \sum_{i\in\{a,b,c\}} \Lambda_{\text{ele},i} + \sum_{j\in\{\omega,v\}} \Lambda_{\text{mech},j}. \quad (9)$$

When Λ crosses a specific user-defined threshold, the fault flag is triggered.

Notice that the frequency sidebands exhibiting the faults are calculated and updated, for each new data window, by using the average mechanical speed value as an input of the FD algorithm. Then, the rotor frequency sidebands are computed using (4) and the definition of f_{r1}.

TABLE III
MULTIPHYSICAL TD AND FD FAULT-DETECTION LOGIC

TD Fault Flag	FD Fault Flag	Log Message
On	On	PEC Failure - Maintenance*
On	Off	Grid Side Problem - Warning
Off	On	Rotor Side Problem - Warning
Off	Off	Healthy Operation

*TD fault isolation is enabled to run.

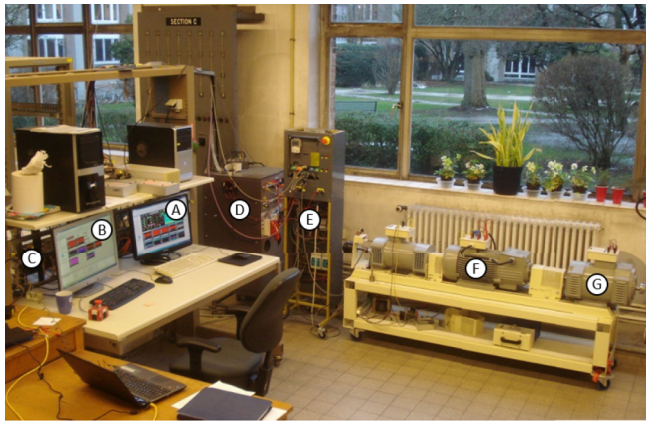

Fig. 5. 3-kW laboratory test bench with (a) dSPACE 1103 and (b) 1104 real-time systems, (c) voltage-source converters in back-to-back topology, (d) monitoring and protecting cabinet, (e) dc drive, (f) DFIG, and (g) dc-machine with independent excitation.

IV. MULTIPHYSICAL TD AND FD FDI TECHNIQUE

The combination of the presented TD and FD techniques increases robustness as the PEC is deemed as faulty only if both techniques detect the fault. RSC faults effectively generate significant oscillation of stator reactive power and electromagnetic torque, as well as rotor frequency sidebands in vibration, mechanical speed, and stator current signals.

However, many other fault types might generate some of the mentioned disturbances, such as grid or rotor imbalance [25], [26]. The former case causes considerable oscillation of the stator reactive power, but no disturbance related to rotor frequency, only triggering the TD technique. On the contrary, the latter case only triggers the FD technique. Therefore, the combined FDI technique provides more than dedicated information to the operator regarding the PEC fault. Table III shows an overview of this logic.

V. EXPERIMENTAL SETUP AND RESULTS

The measurements have been conducted on the 3-kW test bench, comprising a 4-pole wound-rotor induction machine, controlled as a DFIG and driven by a dc machine with independent excitation emulating the aerodynamic torque of a 3.5-kW WT (see Fig. 5). The electrical diagram of the bench is shown in Fig. 6 with voltage, current, rotor-position, and acceleration measurements. The DFIG-rated characteristics and equivalent-circuit parameters can be seen in Tables IV and V.

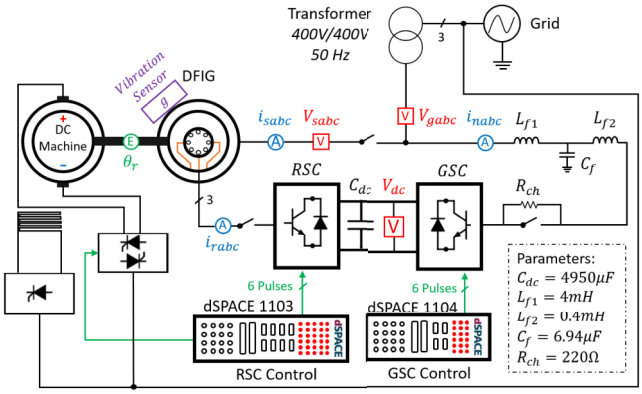

Fig. 6. Electrical diagram of the 3-kW DFIG test bench.

TABLE IV
DFIG-RATED CHARACTERISTICS

Parameters	Values
Power	3000 W
Stator Voltage	230/400 V
Rotor Voltage	130 V
Stator Current	10.7/6.2 A
Rotor Current	20 A
Rated Speed	1385 r/min
Moment of Inertia (J)	0.1153 kgm^2
Friction Coefficient (D)	0.00731 Nms

TABLE V
DFIG EQUIVALENT-CIRCUIT PARAMETERS

Parameters	Values
Stator Resistance (R_s)	1.665 Ω
Rotor Resistance (R'_r)	2.685 Ω
Stator Leakage Inductance (L_{ls})	11.76 mH
Rotor Leakage Inductance (L'_{lr})	11.76 mH
Rated Mutual Inductance (L_m)	279 mH

The rotor and GSCs are switching at 15 and 5 kHz and controlled by a dSPACE 1103 and 1104 fast-prototyping interfaces, respectively. The dSPACE 1103 hardware also sends the torque/speed set-point to a commercial four-quadrant drive, which controls the dc machine.

The DFIG control provides two degrees of freedom for each converter and is illustrated in Fig. 7. The GSC maintains the dc-link voltage at 700 V by ensuring active power balance with the grid and also allow for reactive power production or consumption if needed. Meanwhile, the RSC controls the DFIG torque or speed and the power factor at stator terminals by imposing an active and reactive power flow at rotor terminals [27]. The GSC control is oriented toward the grid voltage angle, rotating, therefore, at synchronous speed, thanks to a phase locked loop [28], while to the RSC control is oriented with the slip angle. The PI controllers used as series compensators are designed based on the modulus optimum and symmetric optimum technique [29], [30].

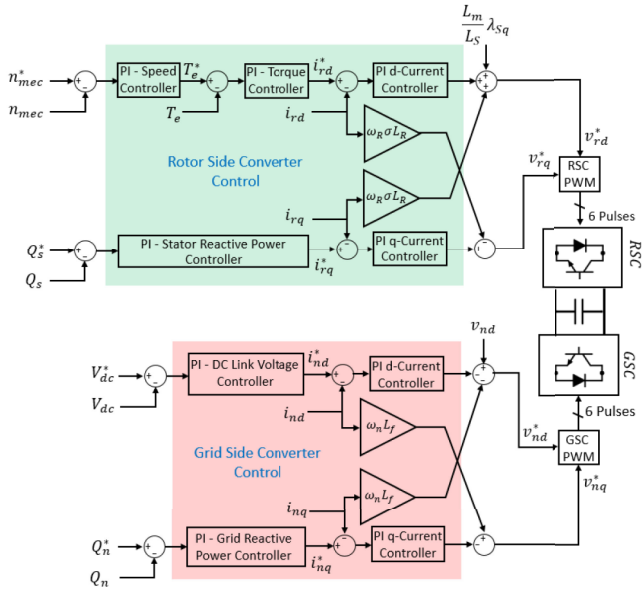

Fig. 7. DFIG schematic control.

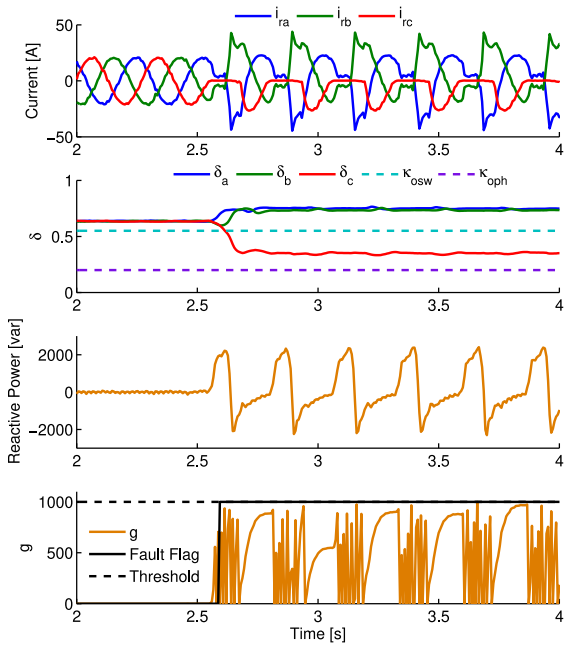

Fig. 8. Experimental results at 1600 r/min, 8 N·m, upper open-switch fault at 2.5 s on phase C. From top to bottom: rotor currents, normalized absolute average current, stator reactive power, and CUSUM output.

A. Validation of the TD FDI

The validation of the TD FDI algorithm is presented in this section for a sampling frequency of 150 Hz. The open-switch-fault case is illustrated in Fig. 8 for unitary power factor at stator terminals. The detection of the fault by the CUSUM algorithm, due to the significant variation of the reactive power, enables the fault isolation algorithm that correctly identifies the faulty IGBT as the top-switch of phase C, according to Table II. The

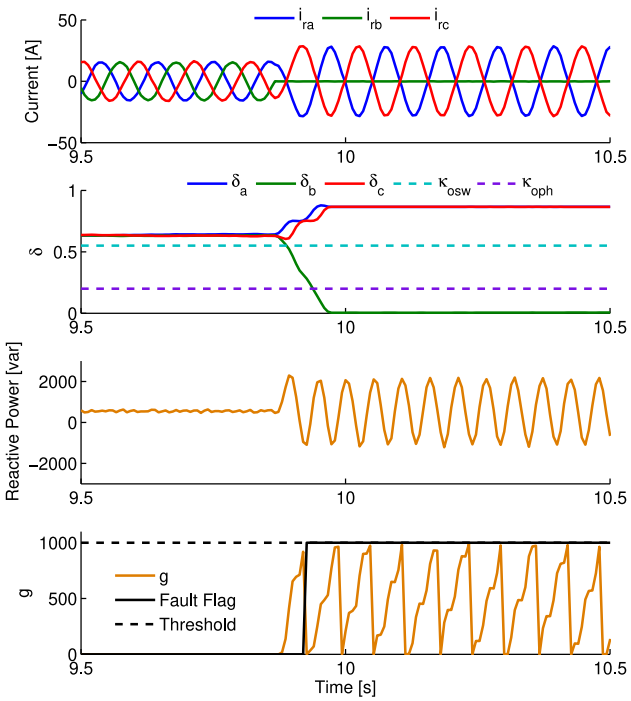

Fig. 9. Experimental results at 1200 r/min, 5 N·m, open-phase fault at 9.9 s on phase B. From top to bottom: rotor currents, normalized absolute average current, stator reactive power, and CUSUM output.

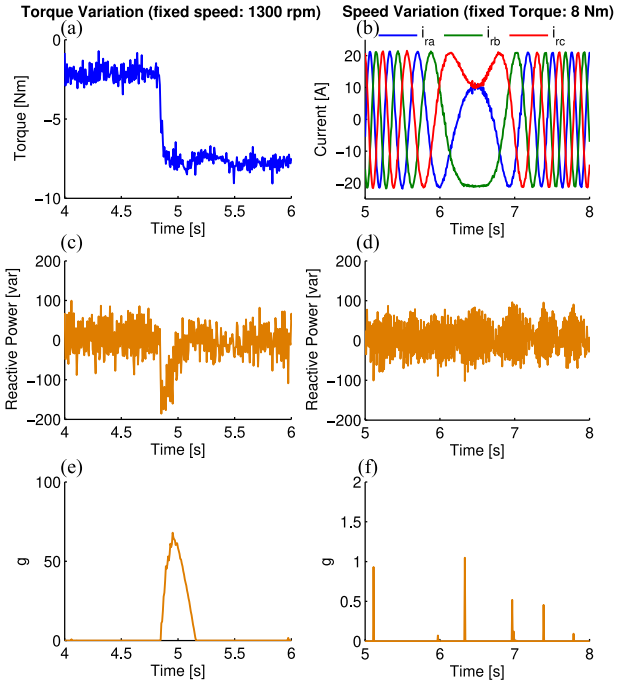

Fig. 10. Experimental results in healthy case, torque step from 2 to 8 N·m (left), speed step from 1300 to 1600 r/min (right). (a) Generator torque. (b) Rotor currents. (c) and (d) Stator reactive power. (e) and (f) CUSUM.

successful detection and isolation of an open-phase fault for 500 var consumed at stator terminals is illustrated in Fig. 9.

The robustness of the algorithm regarding speed and load variation is shown in the left and right parts of Fig. 10, respectively. In each case, the RSC is working in healthy condition. The load and speed variations induce a temporary and limited rise of the CUSUM function, which, however, remains far below the threshold. The fault-isolation algorithm is, therefore, not triggered and the robustness of the algorithm during transient cases is validated, as step variations are furthermore not likely to occur in normal WT operation.

B. Validation of the FD Fault Detection

The validation of the FD fault detection algorithm is presented in this section for a sampling frequency and a resolution of the rectangular time-window equal to 5 kHz and 8192 points (2^{13}), equivalent to 1.64 s, respectively. The open-switch-fault case is illustrated in Fig. 11, showing the rise of the electrical and mechanical fault indicators (d), (e), and (f) as soon as the fault is present. Similar observations can be made in case of open-phase fault in Fig. 12. According to (9), the same weight is used on electrical and mechanical fault indicators to compute the global one. In both cases, the proposed FD fault detection algorithm is able to detect the fault upon occurrence and the fault flag is reset upon clearance.

C. Validation of the Combined FDI

The reaction of both detection techniques for an open-switch fault occurring during a reproduced WT operation (for 500 var consumed at stator terminals) are depicted in Figs. 13 and 14. The sampling frequencies are 150 and 2 kHz for the TD and FD

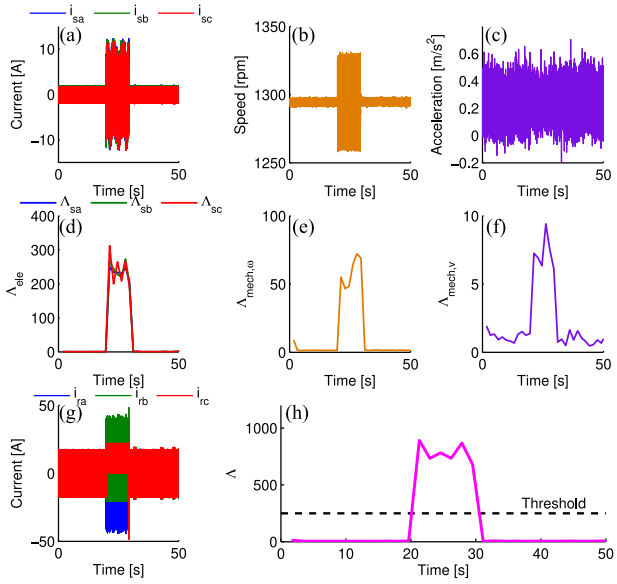

Fig. 11. Experimental results at 1295 r/min, 8 N·m, lower open-switch fault from 19.8 to 29.4 s on phase C. (a) Stator currents, (b) generator speed, (c) vibration signal, FD fault indicators based on (d) stator currents (electrical fault), (e) generator speed and (f) generator vibration (mechanical fault), (g) rotor currents, and (h) sum of FD indicators.

fault detection techniques, respectively. The resolution of the time-window is set to 2048 points (2^{11}), equivalent to 1.02 s. As shown in both figures, the algorithm is able to detect and locate the faulty IGBT in spite of the varying working conditions and the flags are reset upon clearance. Furthermore, no false alarm is generated during healthy conditions.

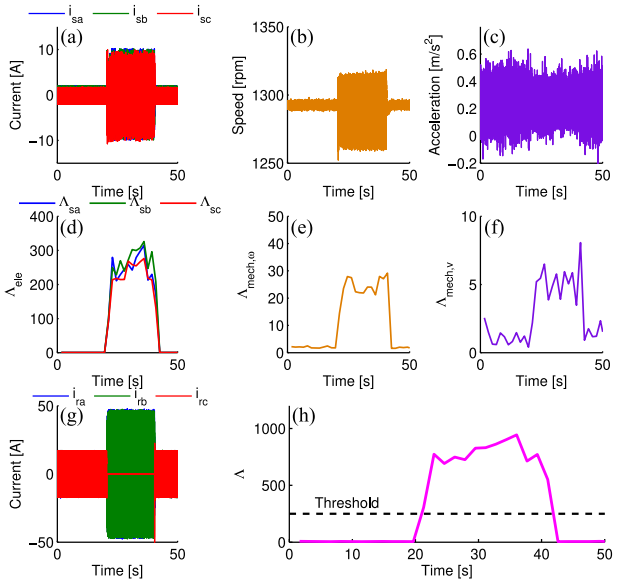

Fig. 12. Experimental results at 1295 r/min, 8 N·m, open-phase fault from 20.6 to 40.5 s on phase C. (a) Stator currents, (b) generator speed, (c) vibration signal, FD fault indicators based on (d) stator currents (electrical fault), (e) generator speed and (f) generator vibration (mechanical fault), (g) rotor currents, and (h) sum of FD indicators.

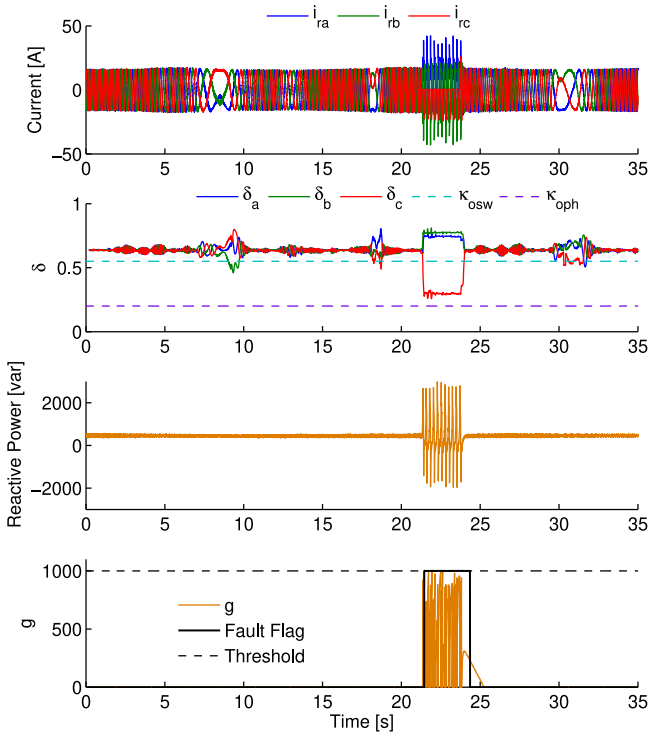

Fig. 13. Experimental results with emulation of dynamic WT operation (speed profile in Fig. 14), upper open-switch fault from 21.2 to 23.78 s on phase C. From top to bottom: rotor currents, normalized absolute average current, stator reactive power, and CUSUM output.

However, the performance of the FD algorithm depends on the resolution of the selected rectangular time window, as depicted in Fig. 15. At constant sampling frequency (5 kHz), a reduction of the size of the rectangular time window affects the frequency

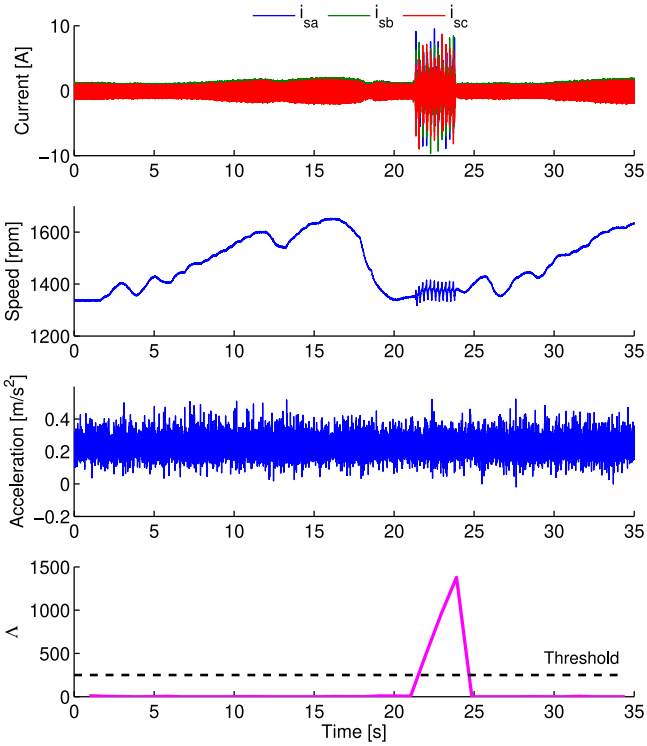

Fig. 14. Experimental results with emulation of dynamic WT operation, upper open-switch fault from 21.2 to 23.78 s on phase C. From top to bottom: stator currents, generator speed, vibration signal and sum of all FD fault indicators.

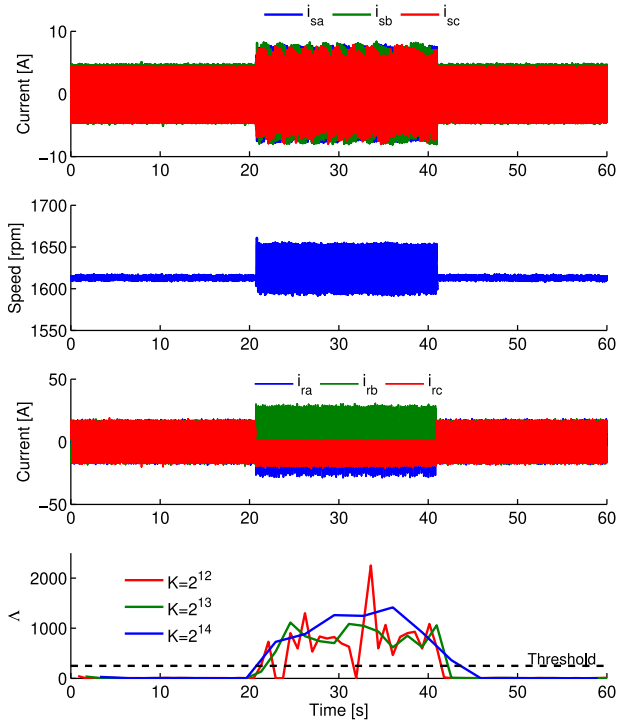

Fig. 15. Experimental results at 1613 rpm, 15 Nm, upper open-switch fault on phase C from 20.7 to 41 s, 5 kHz of sampling frequency with various rectangular window sizes K. From top to bottom: stator currents, generator speed, rotor currents, and sum of all FD fault indicators.

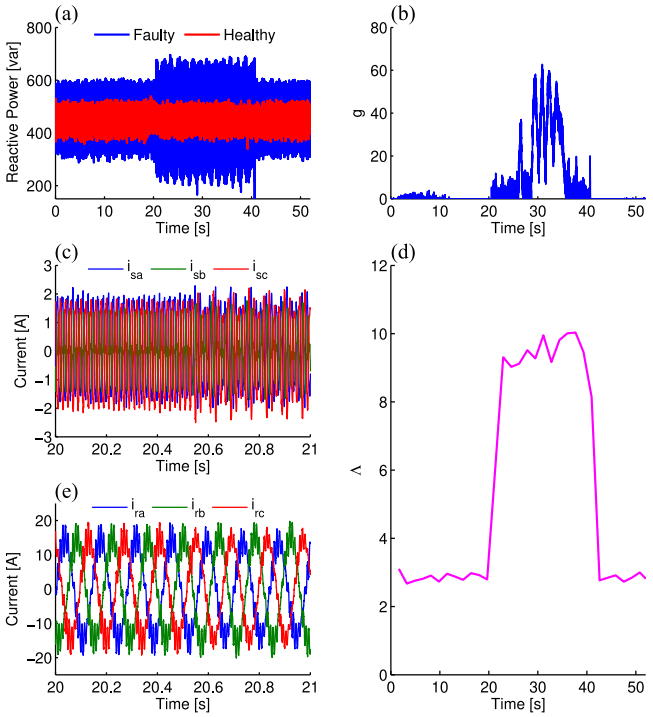

Fig. 16. Experimental results at 1286 rpm, 8 Nm, with grid (continuous) and rotor unbalance (from 20.5 to 41 s): (a) stator reactive power; (b) CUSUM; (c) stator currents; (d) sum of all FD fault indicator; (e) rotor currents.

resolution responsible for identifying the faulty frequency sidebands and can lead to misdetection or false alarms. The global detection variable Λ temporary goes below the threshold in spite of the presence of the fault for the case of the 2^{12} point window. Nevertheless, 2^{13} and 2^{14} point windows lead to a less oscillating and more reliable signal profile for detection.

The sensitivity of the proposed algorithm to grid and rotor unbalance is investigated in Fig. 16. The voltage magnitude of phase A is permanently reduced by 10% at the point of common coupling by adjusting the positions of the jumpers of the supply transformer while a 2.5 Ω resistance is inserted for a defined time in phase C between RSC and rotor terminals, using a bypass circuit-breaker. The rectangular window size and sampling frequency are set to 2^{13} points and 5 kHz, respectively. Before rotor unbalance is applied, the grid unbalance generates a slight increase in the standard deviation of the stator reactive power and a small rise of the CUSUM far below the threshold. On the contrary, the FD detection algorithm is not affected since no rotor-frequency-related sideband is excited. When the rotor unbalance is further applied, the CUSUM further increases, as well as Λ, but both decision functions remain distant from their thresholds. In that case, an intermediate threshold for Λ can be defined in order to inform a rotor unbalance degradation as a predictive maintenance strategy.

VI. Conclusion

A combined TD and FD multiphysical FDI technique for PEC in DFIG WTs, with emphasis on the RSC, has been presented. However, the results and implementation should also carry over to the GSC. Merging the exploitation of the electrical and the mechanical signals increases the reliability of the fault-detection process and allows distinguishing converter faults from other phenomena like grid or rotor imbalance. The ability of the proposed FDI algorithm to detect and locate open-circuit faults in the PEC has been validated through experimental results for different WT operating points.

Throughout this article, the flexibility of the algorithm regarding different sampling frequencies and lengths of the rectangular time-window have been considered. A too low sampling frequency or time-window length may compromise the frequency resolution, the rapidity of the detection, and the correct isolation of the fault. Since computational cost and the availability of high-sampling-rate data are one of the main concerns for industry nowadays, this will be further investigated in future work in order to achieve an optimal tradeoff among low-cost and reliable FDI technique.

VI. Acknowledgment

The authors gratefully acknowledge ENGIE Benelux for the support of the project entitled “Low cost monitoring of WTs (LoCoMot).” Besides, they would like to thank the members of the team dealing with wind farm monitoring for stimulating discussions.

References

[1] E. Artigao, A. Honrubia-Escribano, and E. Gomez-Lazaro, “Current signature analysis to monitor DFIG wind turbine generators: A case study,” *Renewable Energy*, vol. 116, pp. 5–14, 2018.

[2] J. Serrano-González and R. Lacal-Arántegui, “Technological evolution of onshore wind turbines—A market-based analysis,” *Wind Energy*, vol. 19, no. 12, pp. 2171–2187, 2016.

[3] W. Qiao and D. Lu, “A survey on wind turbine condition monitoring and fault diagnosis—Part I: Components and subsystems,” *IEEE Trans. Ind. Electron.*, vol. 62, no. 10, pp. 6536–6545, Oct. 2015.

[4] U. Choi, “Studies on IGBT module to improve the reliability of power electronic systems,” Dept. Energy Technol. Power Electron. Syst., Aalborg Univ. Press, Aalborg, Denmark, 2016.

[5] U.-M. Choi and F. Blaabjerg, “Separation of wear-out failure modes of IGBT modules in grid-connected inverter systems,” *IEEE Trans. Power Electron.*, vol. 33, no. 7, pp. 6217–6223, Jul. 2018.

[6] S. Bęczkowski, P. Ghimre, A. R. de Vega, S. Munk-Nielsen, B. Rannestad, and P. Thøgersen, “Online Vce measurement method for wear-out monitoring of high power IGBT modules,” in *Proc. 15th Eur. Conf. Power Electron. Appl.*, 2013, pp. 1–7.

[7] H. Zhao and L. Cheng, “Open-circuit faults diagnosis in back-to-back converters of DF wind turbine,” *IET Renewable Power Gener.*, vol. 11, no. 4, pp. 417–424, 2017.

[8] N. M. Freire, J. O. Estima, and A. J. M. Cardoso, “Open-circuit fault diagnosis in PMSG drives for wind turbine applications,” *IEEE Trans. Ind. Electron.*, vol. 60, no. 9, pp. 3957–3967, Sep. 2012.

[9] P. Duan, K.-G. Xie, L. Zhang, and X. Rong, “Open-switch fault diagnosis and system reconfiguration of doubly fed wind power converter used in a microgrid,” *IEEE Trans. Power Electron.*, vol. 26, no. 3, pp. 816–821, Mar. 2011.

[10] I. Jlassi, J. O. Estima, S. K. El Khil, N. M. Bellaaj, and A. J. M. Cardoso, “Multiple open-circuit faults diagnosis in back-to-back converters of PMSG drives for wind turbine systems,” *IEEE Trans. Power Electron.*, vol. 30, no. 5, pp. 2689–2702, May 2015.

[11] A. Ismail, L. Saidi, and M. Sayadi, “An open circuit switching fault diagnosis approach for back-to-back converter using wavelet analysis,” in *Proc. 10th Int. Renewable Energy Congr.*, 2019, pp. 1–6.

[12] R. B. Randall, *Vibration-Based Condition Monitoring: Industrial, Aerospace and Automotive Applications*. Hoboken, NJ, USA: Wiley, 2011.

[13] D. Zappalá, N. Sarma, S. Djurović, C. Crabtree, A. Mohammad, and P. Tavner, “Electrical & mechanical diagnostic indicators of wind turbine induction generator rotor faults,” *Renewable energy*, vol. 131, pp. 14–24, 2019.

[14] G. Abad, J. Lopez, M. Rodriguez, L. Marroyo, and G. Iwanski, *Doubly Fed Induction Machine: Modeling and Control for Wind Energy Generation*. Hoboken, NJ, USA: Wiley, 2011, vol. 85.
[15] W. Sae-Kok and D. Grant, "Open switch fault diagnosis for a doubly-fed induction generator," in *Proc. 7th Int. Conf. Power Electron. Drive Syst.*, 2007, pp. 131–138.
[16] M. Basseville and I. V. Nikiforov, *Detection of Abrupt Changes: Theory and Application*. Englewood Cliffs, NJ, USA: Prentice-Hall, 1993, vol. 104, ch. 5.
[17] M. Gálvez-Carrillo and M. Kinnaert, "Sensor fault detection and isolation in doubly-fed induction generators accounting for parameter variations," *Renewable Energy*, vol. 36, no. 5, pp. 1447–1457, 2011.
[18] M. Basseville, "Edge detection using sequential methods for change in level—Part II: Sequential detection of change in mean," *IEEE Trans. Acoust., Speech, Signal Process.*, vol. ASSP-29, no. 1, pp. 32–50, Feb. 1981.
[19] M. Blanke, M. Kinnaert, J. Lunze, M. Staroswiecki, and J. Schröder, *Diagnosis and Fault-Tolerant Control*. Berlin, Germany: Springer, 2006, vol. 2.
[20] J. O. Estima and A. J. M. Cardoso, "A new approach for real-time multiple open-circuit fault diagnosis in voltage-source inverters," *IEEE Trans. Ind. Appl.*, vol. 47, no. 6, pp. 2487–2494, Nov./Dec. 2011.
[21] M. N. Soares, J. Gyselinck, Y. Mollet, C. Peeters, N. Gioia, and J. Helsen, "Vibration-based rotor-side-converter open-switch-fault detection in DFIGs for wind turbines," in *Proc. IEEE Int. Conf. Prognostics Health Manage.*, 2018, pp. 1–6.
[22] R. B. Randall and J. Antoni, "Rolling element bearing diagnostics—A tutorial," *Mech. Syst. Signal Process.*, vol. 25, no. 2, pp. 485–520, 2011.
[23] R. Lyons, "Digital envelope detection: The good, the bad, and the ugly [tips and tricks]," *IEEE Signal Proc. Mag.*, vol. 34, no. 4, pp. 183–187, Jul. 2017.
[24] MathWorks, *Envelope Detection*. 2020. [Online]. Available: https://www.mathworks.com/help/dsp/examples/envelope-detection.html
[25] D. Sun, X. Wang, H. Nian, and Z. Zhu, "A sliding-mode direct power control strategy for DFIG under both balanced and unbalanced grid conditions using extended active power," *IEEE Trans. Power Electron.*, vol. 33, no. 2, pp. 1313–1322, Feb. 2018.
[26] S. Djurović, D. Vilchis-Rodriguez, and A. Smith, "Vibration monitoring for wound rotor induction machine winding fault detection," in *Proc. 20th Int. Conf. Elect. Mach.*, 2012, pp. 1906–1912.
[27] Y. Mollet, "Fault-tolerance and noise and vibration aspects of electrical drives: Application to wind turbines and electrical vehicle traction," BEAMS Dept., Université Libre de Bruxelles, Brussels, Belgium, 2017.
[28] L. G. B. Rolim, D. R. da Costa, and M. Aredes, "Analysis and software implementation of a robust synchronizing PLL circuit based on the PQ theory," *IEEE Trans. Ind. Electron.*, vol. 53, no. 6, pp. 1919–1926, Dec. 2006.
[29] S. M. Tripathi, A. N. Tiwari, and D. Singh, "Optimum design of proportional-integral controllers in grid-integrated PMSG-based wind energy conversion system," *Int. Trans. Elect. Energy Syst.*, vol. 26, no. 5, pp. 1006–1031, 2016.
[30] F. Fröhr and F. Orttenburger, *Introduction to Electronic Control Engineering*. London, U.K.: Heyden, 1982.

Marcelo Nesci Soares (Member, IEEE) received the B.Sc. and M.Sc. degrees in electrical engineering from the Federal University of Rio de Janeiro, Rio de Janeiro, Brazil, in 2015 and 2017, respectively. He is currently working toward the Ph.D. degree with the Bio, Electro, and Mechanical System Department, Université Libre de Bruxelles, Brussels, Belgium, and with the Acoustic & Vibration Research Group, Vrije Universiteit Brussels, Brussels, in collaboration with ENGIE company.

He is currently a Professor with the Federal Center of Technological Education "Celso Suckow da Fonseca" (CEFET/RJ), Rio de Janeiro, Brazil. His main research interests include control of electrical drives, electric machines, power systems protection, power electronics, operation and maintenance, and renewable energy.

Yves Mollet (Member, IEEE) received the master's degree in industrial engineering from the Haute Ecole Léonard de Vinci (ECAM), Brussels, Belgium, in 2010, and the Ph.D. degree in engineering sciences and technology from the Université Libre de Bruxelles (ULB), Brussels, Belgium, in 2017.

He is currently a Researcher with the ULB and with Siemens Industry Software, Leuven, Belgium. His main research interests include identification, modeling, testing, control, fault detection, and noise, vibration and harshness (NVH) aspects of electrical machines and drives.

Michel Kinnaert (Member, IEEE) received the graduate degree from the Université Libre de Bruxelles (ULB), Brussels, Belgium, in 1983, the M.S. degree in electrical engineering from Stanford University, Stanford, CA, USA, in 1984, and the Ph.D. degree from ULB, in 1987.

He was a Research Fellow and a Research Associate of the Fund for Scientific Research from 1984 to 1990. He did a postdoctoral stay with the Department of Electrical Engineering and Computer Science, University of Newcastle, Australia, and held two visiting professor positions with LAGEP, Université Claude Bernard Lyon 1, Lyon, France. He is currently a Full Professor and the Director of the Department of Control Engineering and System Analysis, ULB. He has coauthored the book *Diagnosis and Fault Tolerant Control* (Springer-Verlag, 3rd edition, 2016). His research interests include fault detection and isolation and fault-tolerant control with applications to the process industries, mechatronic systems, as well as energy storage and production.

Dr. Kinnaert is also an Associate Editor for *Control Engineering Practice*. He was the Chairman of the SAFEPROCESS Technical Committee of the International Federation of Automatic Control from 2002 to 2008.

Johan Gyselinck (Member, IEEE) received the M.Sc. and Ph.D. degrees in electromechanical engineering from the Ghent University, Ghent, Belgium, in 1991 and 2000, respectively.

From 2000 to 2004, he was a Postdoctoral Researcher and a Lecturer with the University of Liège, Belgium. Since 2004, he has been a Professor with the Université Libre de Bruxelles, Brussels, Belgium. His main teaching and research topics include low-frequency numerical magnetics, electrical machines and drives, and renewables (wind and photovoltaics).

Jan Helsen (Member, IEEE) received the M.Sc. degree in electromechanical engineering and the Ph.D. degree, focusing on the dynamic simulation of wind turbine gearboxes, from Katholieke Universiteit Leuven, Leuven, Belgium, in 2007 and 2012, respectively.

He is currently a Professor with the Acoustics and Vibrations Research Group, Vrije Universiteit Brussel, Brussel, Belgium. His current research interests include condition monitoring of rotating machines and power systems.